npg

ORIGINAL ARTICLE

Characterization of the genome-wide TLX1 binding profile in T-cell acute lymphoblastic leukemia

K Durinck[1], W Van Loocke[1], J Van der Meulen[1], I Van de Walle[2], M Ongenaert[1], P Rondou[1], A Wallaert[1], CE de Bock[3], N Van Roy[1], B Poppe[1], J Cools[3], J Soulier[4], T Taghon[2], F Speleman[1] and P Van Vlierberghe[1]

The TLX1 transcription factor is critically involved in the multi-step pathogenesis of T-cell acute lymphoblastic leukemia (T-ALL) and often cooperates with NOTCH1 activation during malignant T-cell transformation. However, the exact molecular mechanism by which these T-cell specific oncogenes cooperate during transformation remains to be established. Here, we used chromatin immunoprecipitation followed by sequencing to establish the genome-wide binding pattern of TLX1 in human T-ALL. This integrative genomics approach showed that ectopic TLX1 expression drives repression of T cell-specific enhancers and mediates an unexpected transcriptional antagonism with NOTCH1 at critical target genes, including *IL7R* and *NOTCH3*. These phenomena coordinately trigger a TLX1-driven pre-leukemic phenotype in human thymic precursor cells, reminiscent of the thymus regression observed in murine TLX1 tumor models, and create a strong genetic pressure for acquiring activating *NOTCH1* mutations as a prerequisite for full leukemic transformation. In conclusion, our results uncover a functional antagonism between cooperative oncogenes during the earliest phases of tumor development and provide novel insights in the multi-step pathogenesis of TLX1-driven human leukemia.

INTRODUCTION

T-cell leukemia homeobox 1 (*TLX1, HOX11*) is a homeobox transcription factor oncogene that is ectopically expressed by chromosomal translocations in a subset of human T-cell acute lymphoblastic leukemia (T-ALL). *TLX1* activation is more prevalent in adult than in pediatric T-ALL and is generally associated with a favorable prognosis.[1] TLX1-driven T-ALLs show a unique gene expression signature related to early cortical thymocytes with corresponding expression of CD1a, CD4 and CD8 surface marker proteins. Initial studies showed that TLX1 could immortalize murine hematopoietic precursors,[2,3] but its leukemic potential has only been fully established using TLX1 transgenic mouse models that develop clonal T-cell malignancies with a long latency.[4,5] These TLX1-induced murine T-cell tumors share common features with human TLX1-positive leukemia, including activation of Notch signaling, loss of the *Bcl11b* tumor suppressor gene and a transcriptional program that disrupts the mitotic checkpoint and induces aneuploidy during T-cell transformation.[4] Of note, Lck-TLX1 transgenic mice present with a pre-leukemic phenotype, in which TLX1-positive T-cell precursors undergo a block in differentiation and show enhanced susceptibility toward apoptosis.[4] The decreased thymus size and reduced cellularity observed in TLX1 transgenic mice corresponds with earlier findings in the human context[6] and might be associated with transcriptional repression of the *TCRα* locus by the TLX1-ETS1-RUNX1 complex.[7]

NOTCH1 is a critical regulator of T-cell development and serves as a prominent oncogene in the biology of T-ALL.[8] Critical NOTCH1 target genes are often co-regulated by a transcription factor complex that contains NOTCH1, ETS1 and RUNX1.[9,10] Notably, binding of this complex regularly occurs near super-enhancer regions[11–13] in the vicinity of genes that are critically involved in normal and malignant T-cell development.[9,10] Activating *NOTCH1* mutations occur in more than half of all T-ALLs,[8] but are particularly prevalent in TLX1-positive human T-ALLs.[14] Moreover, *Notch1* mutations are almost uniformly identified in murine T-cell tumors that developed from TLX1 transgenic mice.[4,5] Therefore, *NOTCH1* activation and aberrant expression of *TLX1* are considered collaborative events in the multi-step pathogenesis of T-ALL. However, the exact molecular mechanisms by which these T-cell specific oncogenes cooperate during malignant T-cell transformation and their functional relationship remains to be established.

Here, we used an integrative genomic approach to study the role of the TLX1 transcription factor oncogene in the multi-step pathogenesis of human T-ALL. Furthermore, we evaluated the functional relationship between the cooperative oncogenes *TLX1* and *NOTCH1* in T-ALL to understand their cooperative mechanism-of-action during T-cell transformation.

MATERIALS AND METHODS

Cell lines

ALL-SIL cells were obtained from the DSMZ cell line repository. Cells were maintained in RPMI-1640 medium (Life Technologies, Carlsbad, CA, USA; catalog number 52400-025) supplemented with 20% fetal bovine serum,

[1]Center for Medical Genetics, Department of Pediatrics and Genetics, Ghent University, Ghent, Belgium; [2]Department of Clinical Chemistry, Microbiology and Immunology, Ghent University, Ghent, Belgium; [3]Laboratory for the Molecular Biology of Leukemia, Center for Human Genetics, KU Leuven and Center for the Biology of Disease, VIB, Leuven, Belgium and [4]Genome Rearrangements and Cancer Laboratory, U944 INSERM, University Paris Diderot and Hematology Laboratory, Saint-Louis Hospital, Paris, France. Correspondence: Dr P Van Vlierberghe, Center for Medical Genetics Ghent (CMGG), Ghent University Hospital, Medical Research Building (MRB), Room 120.032, De Pintelaan 185, Ghent 9000, Belgium.
E-mail: pieter.vanvlierberghe@ugent.be
Received 13 February 2015; revised 15 May 2015; accepted 9 June 2015; accepted article preview online 25 June 2015; advance online publication, 17 July 2015
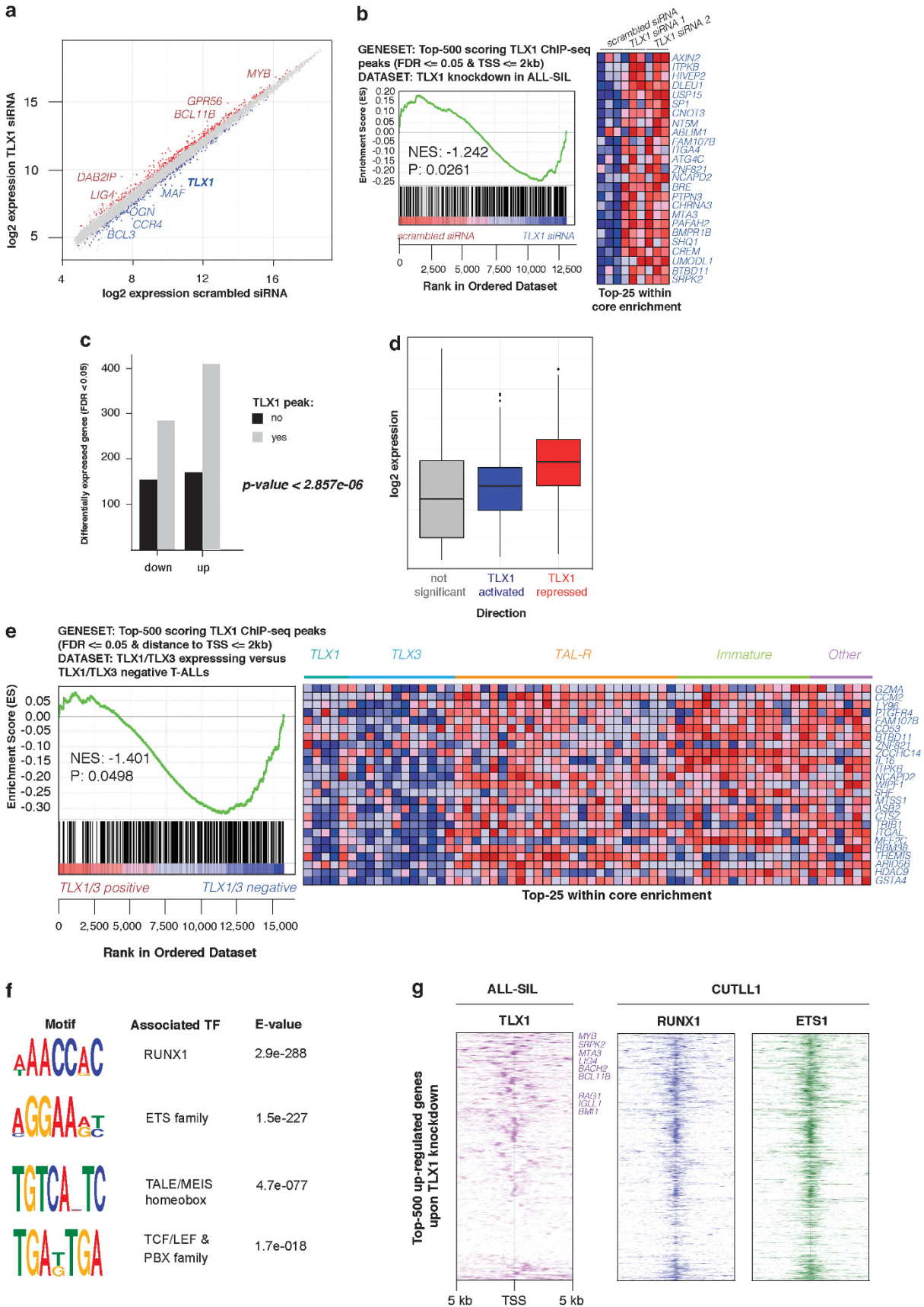
1% of L-glutamine (Life Technologies, 15140-148) and 1% penicillin/streptomycin (Life Technologies, 15160-047).

Clinical samples

Bone marrow lymphoblast samples from 64 T-ALL patients (15 immature, 25 TAL/LMO, 17 TLX1/TLX3 and 7 HOXA) were collected with informed consent according to the declaration of Helsinki from Saint-Louis Hospital (Paris, France) and the study was approved by the Institut Universitaire d'Hématologie Institutional Review Board. This primary T-ALL cohort was previously investigated and the high-quality RNA samples from this cohort were used for gene expression profiling.[15] Gene expression data are accessible on ArrayExpress under accession no. E-MTAB-593.[15]

SiRNA-mediated knockdown, RNA isolation, cDNA synthesis and RT-qPCR

ALL-SIL cells were electroporated (250 V, 1000 μF) using a Genepulser Xcell device (Bio-Rad, Hercules, CA, USA) with 400 nM of Silencer Select Negative Control 1 siRNA (Ambion, #AM4635) or siRNAs targeting TLX1 (Silencer Select, Ambion, Carlsbad, CA, USA; #4392420, s6746 and s6747). ALL-SIL cells were collected 24 h post electroporation. Total RNA was isolated using the miRNeasy mini kit (Qiagen, Venlo, The Netherlands) with DNA digestion on-column. By means of spectrophotometry, RNA concentrations were measured (Nanodrop 1000) and RNA integrity was evaluated (Experion, Bio-Rad). Next, cDNA synthesis was performed using the iScript cDNA synthesis Kit (Bio-Rad) followed by RT-qPCR using the LightCycler 480 (Roche, Vilvoorde, Belgium). Finally, qPCR data were analyzed according to the ΔΔCt-method using the qBasePLUS software (Biogazelle, Zwijnaarde, Belgium).

Western blotting

SDS-PAGE was performed according to standard protocols. For immunoblotting, following antibodies were used: rabbit polyclonal antibody to TLX1 (1:500, Santa Cruz Biotechnology, Dallas, TX, USA; sc-880), mouse monoclonal antibody to alpha-tubulin (1:2000, Sigma-Aldrich, Saint Louis, MO, USA; T5168), mouse monoclonal antibody to beta-actin (1:2000, Sigma-Aldrich, A2228), rabbit polyclonal antibody to ICN1 (1:1000, Cell Signaling, Danvers, MA, USA; Val1744) and rabbit polyclonal antibody to c-MYC (1:500, Santa Cruz Biotechnology, sc-764 (N-262)). Protein level quantification was performed using the ImageJ software (NIH, Bethesda, MD, USA).

Microarray-based gene expression profiling

RNA samples from ALL-SIL cells as well as CD34+ thymus precursor cells were profiled on a custom-designed Agilent micro-array covering all protein coding genes (33,128 mRNA probes, Human Sureprint G3 8x60k micro-arrays (Agilent, Santa Clara, CA, USA)) and 12 000 lncRNAs (23 042 unique lncRNA probes).[16] Expression data were normalized using the VSN-package (Bioconductor release 2.12) in R. Differential expression analysis was performed in R using Limma. All gene expression profiling data have been deposited in the GEO database (GSE62144).

Compound treatment of T-ALL cell lines

ALL-SIL cells were seeded at a density of 1×10^6 cells/ml and treated for 12 h with either DMSO or 1 μM of JQ1 compound (BPS Bioscience, San Diego, CA, USA; catalog number 27401). ALL-SIL cells were seeded at a density of 1×10^6 cells/ml and treated for 48 h with either DMSO or 1 μM of compound E (Enzo Life Sciences, Antwerp, Belgium; catalog number ALX-270-415-C-250). Cells were harvested at the indicated time points and RNA isolation was performed as described above.

ChIP-seq and ChIP-qPCR

The ChIP-protocol has been adapted from previous studies.[17] In brief, 1×10^7 cells were cross-linked with 1.1% formaldehyde (Sigma-Aldrich, F1635) at room temperature for 10 min and the cross-linking reaction was quenched with glycine (125 mM final concentration, Sigma-Aldrich, G-8790). Nuclei were isolated and chromatin was purified by chemical lysis. Next, the purified chromatin was fragmented to 200–300 bp fragments by sonication (Covaris, Woburn, MA, USA; S220, Focused-ultrasonicator). Chromatin immunoprecipitation was performed by incubation of the chromatin fraction overnight with 100 μl of protein-A coated beads (Thermo-Scientific, Waltham, MA, USA; catalog number 53139) and 10 μg of fibrillarin-specific (Abcam, Cambridge, UK; ab5821), H3K27ac-specific antibody (Abcam, ab4729) or TLX1-specific antibody (Santa-Cruz Biotechnology, sc-880). The next day, beads were washed to remove non-specific binding events and enriched chromatin fragments were eluted from the beads, followed by reverse cross-linking by incubation at 65 °C overnight. DNA was subsequently purified by phenol/chloroform extraction, assisted by phase lock gel tubes (5Prime). DNA obtained from the ChIP assays was adaptor ligated, amplified and analyzed by Illumina Hiseq 2000 (Illumina, San Diego, CA, USA). Raw sequencing data were mapped to the human reference genome (GRCh37/h19) using Bowtie.[18] Peak calling was performed using MACS 1.4.[19] ChIP seq data have been deposited in the GEO database (GSE62144).

Relative real-time PCR quantification of promotor sequences was normalized to HPRT1 DNA levels (negative control region) in chromatin immunoprecipitates performed with TLX1-specific antibody (Santa Cruz Biotechnology, sc-880, rabbit polyclonal antibody) or fibrillarin-specific antibody (negative control antibody) (Abcam, ab5821, rabbit polyclonal antibody). Additionally, real-time PCR quantification was normalized in chromatin immunoprecipitates performed with a RUNX1 (Abcam, ab92336, rabbit monoclonal antibody) and ETS1 (Cell signaling, 6258 S, rabbit polyclonal antibody) specific antibodies to immunoprecipitation with a fibrillarin-specific antibody. ChIP-qPCR primers for CHEK1, BUB1, BCL11B and BRCA2 were used as described previously.[4] Enrichment was calculated using the ΔΔCt method.

Motif enrichment

A TLX1 peak multi-fasta file (500 bp centered around the peak summits) was produced using BedTools[20] and was subsequently submitted to the MEME-ChIP[21] public server for motif enrichment analysis. This motif analysis was performed on the top quartile (25% of the highest scoring) of TLX1 ChIP-seq peaks. The 'fasta-get-markov' module, included in the MEME suite, was used to create a background model based on all TLX1 peaks as called by MACS1.4.

ChIP-seq peak heatmaps

Public ChIP-seq data for ETS1, RUNX1, ICN1 and BRD4 in CUTLL1[9] were downloaded from GEO series GSE51800. Fastq files were aligned to the reference genome (hg19) with Bowtie. HOMER[22] was used to produce tag directories and heatmap data matrices of public ChIP-seq data and TLX1 ChIP-seq data. Heatmaps were produced in R. TSS-centered heatmaps were ordered based on average linkage clustering of the rows in the TLX1 heatmap. TLX1 ChIP-seq peak heatmaps were ordered by descending TLX1 peak heights.

Thymocyte transduction and culturing on OP9-DLL1

Pediatric thymus samples were obtained and used according to the guidelines of the Medical Ethical Commission of the Ghent University Hospital (Belgium). CD34+ thymocytes were purified using magnetic activated cell sorting (Miltenyi Biotec, Leiden, The Netherlands) and cultured for 24 h in complete IMDM, supplemented with penicillin (100 U/ml),

---

Figure 1. Characterizing the genome-wide TLX1 binding pattern. (**a**) Scatter plot showing significantly down- (blue) and upregulated (red) genes (P-adj. value < 0.05) upon TLX1 knockdown in ALL-SIL leukemic cells, (**b**) GSEA shows a significant enrichment of the top-500 scoring (FDR < 0.05) TLX1 binding sites in proximity (⩽2 kb) of the TSS among the TLX1 repressed genes, (**c**) Barplot showing the distribution of TLX1 ChIP-seq peaks between genes up- or downregulated upon TLX1 knockdown in ALL-SIL, (**d**) Boxplot showing that TLX1 repressed genes have a higher average expression level in comparison with genes either activated by TLX1 or not differentially expressed upon TLX1 knockdown in ALL-SIL, (**e**) Validation of the same geneset as defined in (**b**) in a primary cohort of 64 T-ALL patients (5 TLX1+ cases and 12 TLX3+ cases), (**f**) MEME-ChIP motif analysis identifies RUNX and ETS family member motifs among the strongest enriched DNA motifs in TLX1 binding sites identified by ChIP sequencing, (**g**) Heatmap representation of ChIP profiles of TLX1 in ALL-SIL cells and ETS1-RUNX1 sites in CUTLL1 cells at the top-500 upregulated genes upon TLX1 knockdown, clustered according to average linkage.

---

streptomycin (100 µg/ml), L-glutamine (2 mM) (all from Invitrogen) and 10% heat-inactivated FCS (Biochrom, Berlin, Germany) in the presence of 10 ng/ml IL-7 and SCF. After 24 h, cells were retrovirally transduced with either LZRS-IRES-EGFP (LIE) or LZRS-TLX1-IRES-EGFP (TLX1) as described previously.[23] For the double transfection experiments, retroviral transduction was performed using either MSCV-mCherry or MSCV-mCherry-TLX1 (TLX1) at 24 h. Next, mCherry^{+} cells were sorted and directly transduced with either MSCV-EGFP or MSCV-EGFP-ICN1 at 48 h. Next, equal numbers of transduced cells were seeded onto confluent OP9-GFP or OP9-DLL1 plates in α-MEM media supplemented with 20% heat-inactivated FCS plus 100 U/ml penicillin, 100 µg/ml streptomycin, 2 mM L-glutamine and the T-lineage supporting cytokines SCF, Flt3-L and IL-7 at 5 ng/ml each. Following 72 h of OP9 co-culture, cells were harvested by forceful pipetting and stained with CD45-PE (Miltenyi) to purify CD45^{+}EGFP^{+}, CD45^{+} mCherry^{+} or CD45^{+}mCherry^{+}EGFP^{+} human transduced leukocytes through sorting to remove contaminating OP9 stromal cells. After sorting, part of the cells were lysed in 700 µl QIAzol (Qiagen) and stored at − 80 °C before RNA isolation, while the other part was used to perform T-cell differentiation experiments as described previously.[24] To evaluate T-cell development, co-cultures were harvested at indicated time points by forceful pipetting, stained with monoclonal antibodies as described previously[24] and analyzed on a LSRII flow cytometer using FACSDiva software (BD Bioscience, San Jose, CA, USA).

Ectopic TLX1 expression in CUTLL1

CUTLL1 cells were seeded at a density of $1 \times 10e6$ cells/ml in RPMI-1640 medium supplemented with 20% fetal bovine serum and retrovirally transduced with either LZRS-IRES-EGFP (control vector) or LZRS-TLX1-IRES-EGFP (TLX1). After 72 h, transduced cells were sorted to purify EGFP^{+} CUTLL1 cells. After sorting, cells were lysed in 700 µl QIAzol (Qiagen) and stored at − 80 °C before RNA isolation.

RESULTS

Genome-wide binding profile of TLX1 in human T-ALL

To identify the genome-wide binding pattern of TLX1 in the context of human T-ALL, we performed chromatin immunoprecipitation followed by sequencing (ChIP-seq) in ALL-SIL, a human T-ALL cell line with ectopic TLX1 expression as a result of the t(10;14)(q24;q11) translocation. This analysis identified 18 187 unique TLX1 binding peaks (FDR < 0.05) with a distribution of 19.8% in the proximity of transcriptional start sites (TSSs) of protein-coding genes, 43.5% in intronic and 36.7% in intergenic regions of the human genome (Supplementary Figure 1a). Notably, genes characterized by the strongest TLX1 binding events showed higher average expression levels as compared with genes with moderate or no TLX1 binding (Supplementary Figure 1b). The validity of our approach was confirmed by ChIP-qPCR analysis of TLX1 binding at promoter regions of previously reported TLX1 targets,[4] including BCL11B, BUB1, CHEK1 and BRCA2 (Supplementary Figure 1c).

To unravel the transcriptional consequences of TLX1 binding, we performed micro-array gene expression analysis before and after TLX1 knockdown in ALL-SIL cells using two independent TLX1 targeting siRNAs (Figure 1a, Supplementary Figures 2a and b). Gene set enrichment analysis (GSEA) confirmed that TLX1 binding peaks (top 500 and top 1000 scoring peaks) located near TSSs of protein-coding genes were significantly enriched in genes upregulated after TLX1 knockdown in ALL-SIL (Figure 1b and Supplementary Figure 2c), in line with the previously recognized role of TLX1 as a transcriptional repressor in T-ALL.[4,25] In addition, this notion was further confirmed by a significantly higher number of TLX1 bound genes that are upregulated as compared with downregulated after TLX1 knockdown (Figure 1c). Notably, the average gene expression levels of targets repressed by TLX1 were higher in comparison with TLX1 activated genes or those that were not significantly differentially expressed upon TLX1 knockdown in ALL-SIL (Figure 1d). Consistent with previous reports, we also obtained a significant enrichment of the TLX1 binding peaks near TSSs in genes that are downregulated in both TLX1 or TLX3

driven primary T-ALLs, in keeping with previously noted overlap between TLX1 and TLX3 transcriptional programs (Figure 1e).[4,25]

Next, we evaluated the presence of co-factor binding sites at TLX1-bound regions by means of motif analysis (Figure 1f). A strong enrichment was found for RUNX family member (E-value: $2.9e - 288$) and ETS transcription factor motifs (E-value: $1.5e - 227$), consistent with previously published data.[7,25] Moreover, but to a lesser extent, we found enrichment for other co-factors previously linked to TLX1 functionality, including MEIS and PBX transcription factor family members.[26,27]

The genome-wide binding profiles of RUNX1 and ETS1 were previously shown to be highly overlapping in the context of T-ALL.[9] Moreover, ETS1 cooperates with TLX1 at the TCRα locus and RUNX1 was shown to act as a central hub in the TLX1 regulatory network.[25] Given this, we integrated our TLX1 ChIP-seq profiles with publically available ETS1 and RUNX1 ChIP-seq data[9] and evaluated the extent of overlap between these transcription factors at the TSSs of genes that are upregulated after TLX1 knockdown in ALL-SIL (that is, bona fide TLX1 repressed target genes). We generated a heatmap of the TLX1 ChIP-seq binding profile for the top-500 genes upregulated upon TLX1 knockdown by clustering of TLX1 ChIP-seq signals within a 10-kb window surrounding the TSS (Figure 1g). Next, ChIP-seq binding profiles for RUNX1 and ETS1 were visualized in the exact same gene order as defined by the TLX1 ChIP-seq data (Figure 1g). Similar and overlapping patterns observed in these ChIP-seq heatmaps support our motif analysis (Figure 1f) and confirm a high degree of overlap between TLX1, ETS1 and RUNX1 binding sites in the promoter of TLX1 repressed genes. To verify whether these overlapping binding patterns between TLX1, RUNX1 and ETS1 also result in a similar transcriptional read-out, we performed siRNA-mediated knockdown for RUNX1 and ETS1 in ALL-SIL. The resulting gene signatures were scored to the transcriptional profile associated with TLX1 inactivation in ALL-SIL by GSEA. This analysis points toward a common transcriptional regulatory network between these three transcriptional regulators (Supplementary Figures 3a and b). Furthermore, ChIP-qPCR analysis in ALL-SIL confirmed direct binding of both RUNX1 and ETS1 at the exact same binding sites as observed for TLX1 at canonical target genes, including BCL11B, CHEK1, BRCA2 and BUB1 (Supplementary Figures 3c and d). Overlapping binding patterns between TLX1, RUNX1 and ETS1 could not be observed using the top-500 downregulated genes upon TLX1 knockdown (Supplementary Figure 4).

TLX1 binding at super-enhancers in human T-ALL

Recently, enhancer sites with broad binding of traditional enhancer associated histone marks (H3K27ac and H3K4me1) and co-occupation of the transcriptional co-activators BRD4 and MED1 were identified.[11,12] These so-called super-enhancers mark the binding sites for transcription factor complexes that establish a unique cell identity program and drive expression of both lineage identity genes as well as prominent oncogenes in human cancer.

Given the role of TLX1 as oncogenic transcriptional repressor, we wondered whether TLX1 could interfere with super-enhancer activity[11,12] in the context of TLX1-driven human leukemia. For this, we performed H3K27ac ChIP-seq analysis in the T-ALL cell line ALL-SIL and used the normalized H3K27ac cluster signals in function of the normalized ranks to identify super-enhancers in this TLX1-driven tumor line, as previously described[12] (Supplementary Figure 5a). Next, we performed a similar analysis based on TLX1 ChIP-seq data and clustered TLX1 peaks within 12.5 kb from each other. These TLX1 clusters were superimposed on the H3K27ac super-enhancer plot, which revealed a large overlap between super-enhancer sites and TLX1 binding clusters in the ALL-SIL genome (Figure 2a). Notably, these top-ranked super-enhancer sites were often located within the vicinity of
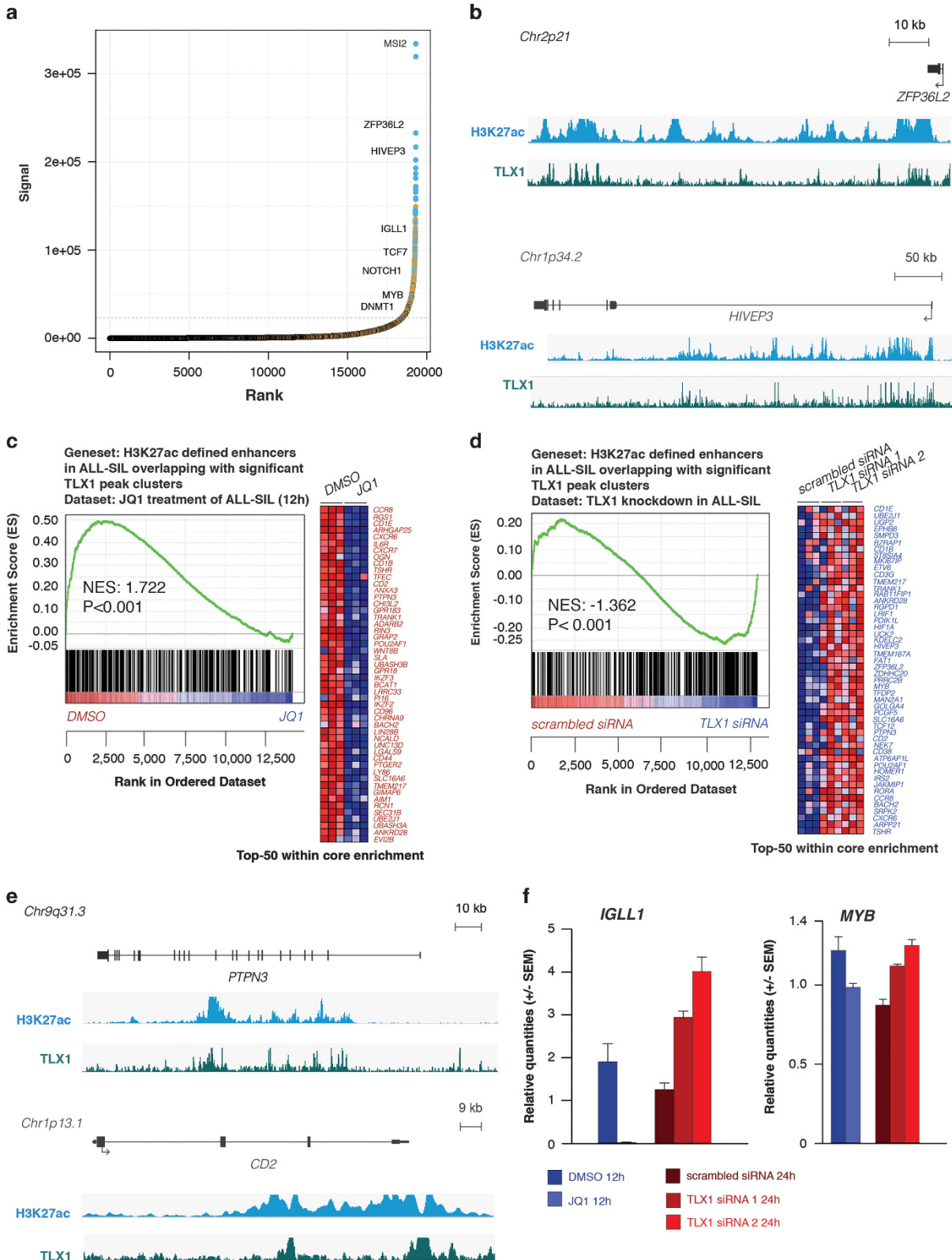
Figure 2. The role of TLX1 at (super)-enhancer sites. (**a**) Hockey-stick plot representing the normalized rank and cluster signal of clusters of H3K27ac peaks (super-enhancers) overlapping with significant TLX1 ChIP-seq peak clusters (blue dots), overlapping with TLX1 binding events that are not organized in significant clusters (orange dots) or not overlapping with TLX1 binding events (black dots), (**b**) Examples of H3K27ac defined super-enhancer sites characterized by large TLX1 ChIP-seq peak clusters within the proximity of *ZFP36L2* and *HIVEP3*, (**c**) GSEA of the top-500 scoring H3K27ac defined super-enhancer sites with significant TLX1 clusters (orange and blue dots from **a**) within the set of genes downregulated by JQ1 in ALL-SIL, (**d**) GSEA of the same geneset as in (**c**) within the set of genes upregulated upon TLX1 knockdown in ALL-SIL, (**e**) Examples of H3K27ac and TLX1 ChIP-seq signals at the *PTPN3* and *CD2* loci, both significantly enriched in the GSEA analyses shown in (**c**) and (**d**), (**f**) Confirmation of *IGLL1* and *MYB* responsiveness to JQ1 treatment and TLX1 knockdown in ALL-SIL by RT-qPCR.

crucial regulators involved in normal and malignant T-cell development, for example *ZFP36L2* and *HIVEP3* (Figure 2b).

To further confirm true super-enhancer identity of TLX1 bound super-enhancer sites, we interrogated their responsiveness to treatment with the small-molecule BET-inhibitor JQ1.[28] Response to treatment was verified by downregulation of *c-MYC* RNA levels (Supplementary Figure 5b) and protein levels (Supplementary Figure 5c). For this, we used micro-array analysis to evaluate the transcriptional response of ALL-SIL cells upon JQ1 treatment (Supplementary Figure 5d). Notably, GSEA showed that H3K27ac defined super-enhancers characterized by co-binding of TLX1 were significantly enriched in genes downregulated upon JQ1 treatment in ALL-SIL (Figure 2c). In addition, the same TLX1 bound super-enhancer sites were significantly enriched for genes that are upregulated upon TLX1 knockdown (suppressed by TLX1; Figure 2d), suggesting that TLX1 interferes with enhancer function at these loci. Notably, the core enrichment for these GSEA analyses included several genes with an established role in either T-cell development (*PTPN3*, *RAG2*, *BACH2*, *HIVEP3*, *CD2*) or T-ALL pathogenesis (*ETV6*, *MYB*) (Figure 2e). The response of these genes to JQ1 treatment or TLX1 knockdown, respectively, was confirmed by RT-qPCR (Figure 2f).

Transcriptional antagonism between the cooperative oncogenes *TLX1* and *NOTCH1*

Previous studies have shown that NOTCH1, ETS1 and RUNX1 define a transcription factor complex that co-regulates important NOTCH1 target genes.[9,10] Moreover, binding of this complex can also occur near super-enhancer regions in the vicinity of genes critically involved in normal and malignant T-cell development.[9] Given that RUNX1 and ETS1 often co-occupy TLX1 binding sites and that TLX1 can also associate with regions of super-enhancer activity, we wondered whether TLX1 could interfere with the transcriptional program mediated by NOTCH1.

To address this issue, we evaluated the relationship between the NOTCH1 transcriptional program and the gene expression signature associated with TLX1 knockdown in ALL-SIL. Surprisingly, GSEA showed that direct NOTCH1 target genes (downregulated upon GSI treatment of ALL-SIL cells;[29] Supplementary Figures 6a–c) were significantly enriched for genes repressed by TLX1 (Figure 3a). TLX1 and ICN1 binding near the *NOTCH3* and *IL7R* loci are shown as representative examples for overlapping binding events of these factors at canonical *NOTCH1* target genes (Figure 3b). Notably, next to some of the canonical NOTCH1 targets also *NOTCH1* itself is upregulated upon TLX1 knockdown in ALL-SIL, at both the mRNA and protein level (Figure 3c). The TLX1-driven repression of some of these NOTCH1 target genes was confirmed upon ectopic *TLX1* expression in the CUTLL1 cell line (as shown for *NOTCH3*; Figure 3d). Interestingly, strong and overlapping binding of TLX1 with NOTCH1 was also observed at the recently identified long-range acting *MYC* enhancer (Figure 3e).[30] Finally, alignment of the genome-wide ICN1, ETS1 and RUNX1 ChIP-seq peaks in CUTLL1 T-ALL cells with those of TLX1 in ALL-SIL cells showed a striking binding overlap for these transcription factors as visualized by ChIP-seq heatmaps (3 kb centered around the TLX1 summits; Figure 3f and Supplementary Figure 6d).

TLX1 broadly interferes with normal T-cell development

Previously, it has been shown that Lck-TLX1 transgenic mice are characterized by reduced thymus size and cellularity as a pre-leukemic phenotype that precedes full leukemic transformation.[4] In addition, enforced *TLX1* expression in human cord blood CD34+ progenitor cells disrupted primary T-cell differentiation and triggered enhanced thymocyte apoptosis.[6] These data suggest that ectopic induction of the *TLX1* oncogene in T-cell precursors negatively affects T-cell differentiation, proliferation and survival.

To further study the role of TLX1 during the initial phases of tumor development, human thymus-derived CD34+ precursor T cells were infected with a retroviral construct that drives ectopic TLX1 expression and cultured on a feeder layer of OP9 stromal cells expressing the NOTCH1 ligand DLL1 (Figure 4a). In line with previous results,[6] ectopic TLX1 expression strongly perturbed normal T-cell development, with a drastic reduction in absolute number of thymocytes as compared with control cells (Figure 4b). Moreover, at day 12 of co-culture, we observed a drastic reduction in CD4+CD8+ double positive (17.1 vs 63.2%) (Figure 4c) as well as CD7+CD1a+ and CD3+ TCRγδ positive (0.7 vs 3.4%) T cells overexpressing TLX1 (Supplementary Figure 7). In line with the transcriptional antagonism between TLX1 and NOTCH1 described above, thymocytes that ectopically express TLX1 also showed a reduction in IL7Rα (CD127) surface expression compared with controls (Figure 4d). Moreover, the previously established enhancer sites downstream of the IL7R locus showed overlapping binding of ETS1, RUNX1, ICN1, BRD4 and TLX1 (Figure 4e).

Cortical thymocyte maturation arrest in TLX1-positive human T-ALL has been linked to TLX1-mediated repression of TCRα enhancer activity and a subsequent block in TCR-Jα rearrangement.[7] Notably, our TLX1 ChIP-seq data confirmed these findings with TLX1 binding at the TCRα enhancer site in the TCRα locus (Figure 4e). However, our data also suggest that TLX1 may be implicated in a more global repression of the T-cell recombination machinery including a broad pattern of TLX1 binding at the TCRα and TCRβ locus (Figure 4e) as well as simultaneous binding near critical regulators of V(D)J-recombination including *RAG1* (Figure 4e).

Furthermore, gene expression profiling analysis of TLX1 over-expressing versus control human CD34+ thymocytes derived from two representative CD34+ donors at 72 hours post transduction confirmed genome-wide antagonistic effects between TLX1 and NOTCH1 in this independent *in vitro* model system. TLX1-driven transcriptional repression of *NOTCH1*, *NOTCH3*, *IL7R*, *IGLL1*, *SHQ1*, *RAG1* and *RAG2* is shown as representative examples (Figure 4f). Moreover, upregulation of some of these genes was also confirmed by RT-qPCR upon TLX1 knockdown in ALL-SIL (Figure 4g).

To further study the functional antagonism between TLX1 and NOTCH1, we verified whether ICN1 would be able to rescue the reduction in cell counts induced by TLX1 ectopic expression in T-cell progenitor cells. To this end, human CD34+ progenitor T cells from three independent donors were sequentially transduced with a TLX1 and/or ICN1 overexpression constructs. Absolute total cell counts were measured 18 and 24 days post transduction (Figure 5). As previously documented, TLX1 over-expression induced a reduction in cell numbers. However and most notably, ICN1 expression rescued this TLX1-driven pheno-type and partially restored cell numbers in these co-culture experiments (Figure 5).

A tumor suppressor network within the TLX1 regulome in T-ALL

Previous studies have shown direct binding of TLX1 in the promoter region of well-established T-ALL tumor suppressor genes,[4,25] including *BCL11B*, *RUNX1* and *WT1*.[4,25] From this, a model emerged in which TLX1-mediated suppression of tumor suppressors would eventually provide genetic pressure toward genomic deletion or mutation of these factors during TLX1-driven transformation.[4,25]

To further expand the tumor suppressor network regulated by TLX1, we evaluated the TLX1 binding pattern near currently known T-ALL tumor suppressor genes. This analysis revealed a broad network of tumor suppressors bound by TLX1 including *TET1*, *EZH2*, *FBXW7*, *PTEN*, *BCL11B*, *FAT1*, *RUNX1*, *LEF1*, *GATA3*, *ETV6*, *WT1*, *PTPN2*, *CDKN1B*, *RB1*, *DNM2*, *CNOT3*, *RPL5*, *RPL10* and *SH2B3* (Figure 6a, Supplementary Figures 8 and 9). In line with other
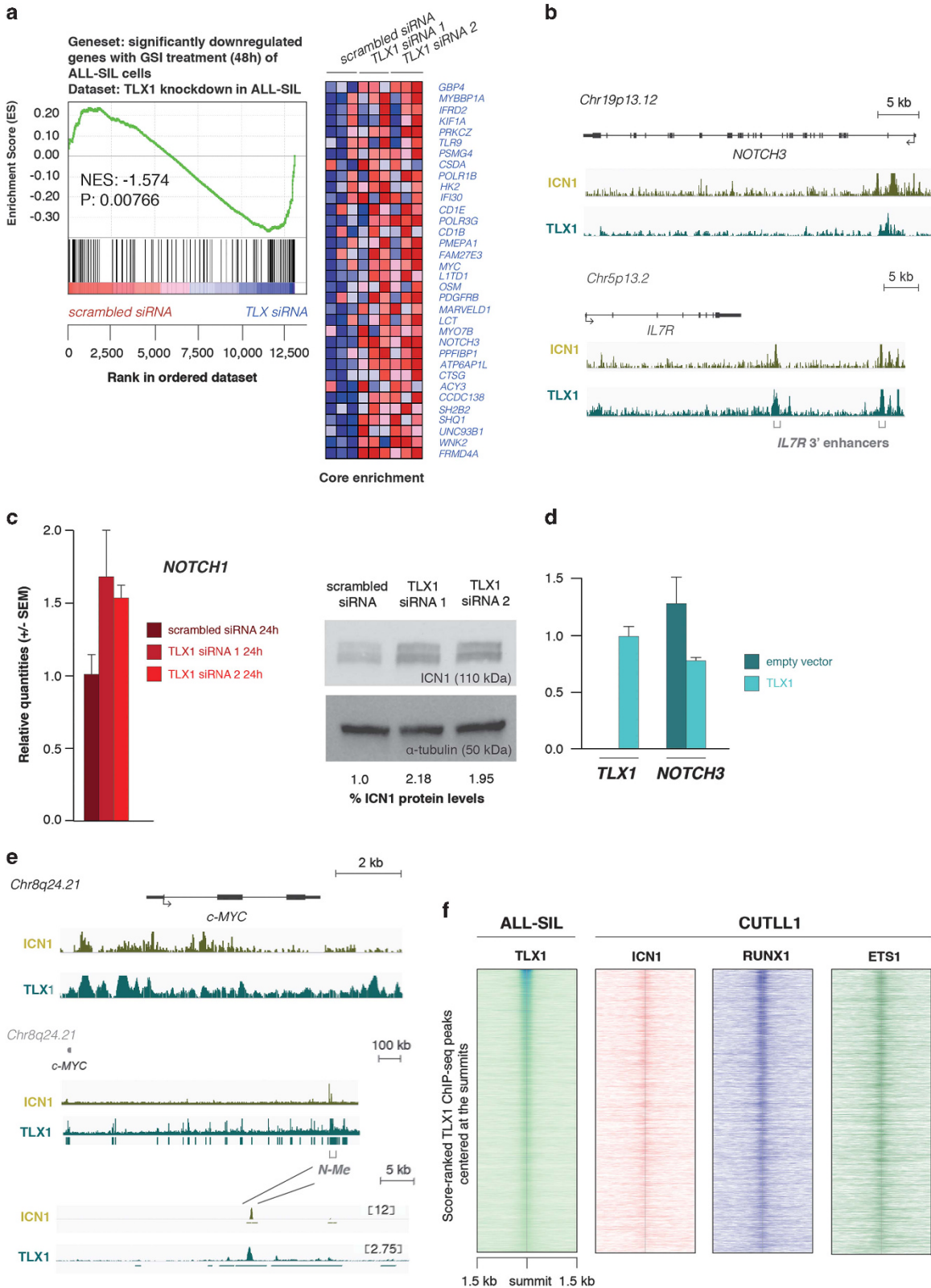
Figure 3. Transcriptional antagonism between cooperative oncogenes NOTCH1 and TLX1 in T-ALL. (a) GSEA shows that the top-500 downregulated genes upon GSI treatment of ALL-SIL T-ALL cells are significantly enriched within the set of genes that are upregulated upon TLX1 knockdown in ALL-SIL, (b) ChIP-seq profiles of ICN1 and TLX1 showing overlapping binding patterns at the canonical NOTCH1 target genes NOTCH3 and IL7R, (c) confirming upregulation of NOTCH1 upon TLX1 knockdown in ALL-SIL cells, (d) Ectopic expression of TLX1 in CUTLL1 leads to reduced expression of the canonical NOTCH1 target gene NOTCH3 as shown by RT-qPCR, (e) ChIP-seq profiles of ICN1 and TLX1 at the NOTCH3 and IL7R loci, (e) ChIP-seq profiles of ICN1 and TLX1 at the genomic region spanning from c-MYC toward its recently described long-range enhancer site[30] and visualization of the high-scoring and overlapping ICN1 and TLX1 peak at this specific enhancer site,[30] (f) Heatmap representation of the ChIP-seq overlap of TLX1-ICN1-ETS1-RUNX1 sites across a genome-wide score-based ranking of TLX1 ChIP-seq signals.
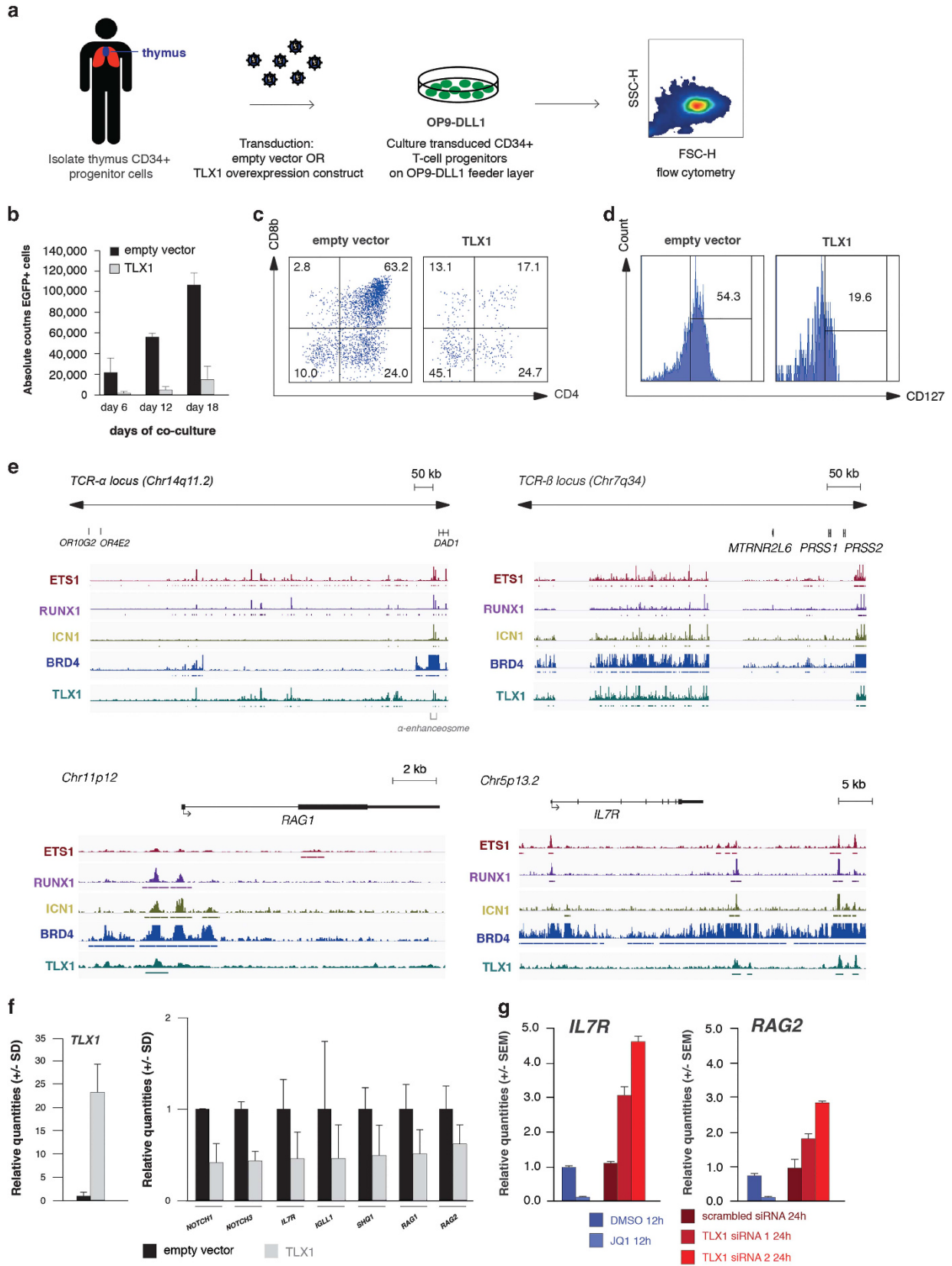
results obtained from the genome-wide TLX1 binding profile, ChIP-seq peaks for ETS1, RUNX1 and ICN1 showed high positional overlap with TLX1 binding sites in the vicinity of these T-ALL tumor suppressor genes as shown for *BCL11B*, *CNOT3*, *ETV6* and *FAT1* (Figure 6a).

Gene expression profiling confirmed upregulation for the majority of these factors upon TLX1 knockdown in ALL-SIL (Figures 6b and c) and was confirmed for *BCL11B* by RT-qPCR analysis (Figure 6c). Although the majority of these tumor suppressors were downregulated upon JQ1 treatment in ALL-SIL (Figure 6d), the strongest and most significant effects were observed for *FAT1*, *WT1* and *ETV6* (Figure 6e), as confirmed by RT-qPCR for *ETV6* (Figure 6e).

DISCUSSION

TLX1 is a driver oncogene in the pathogenesis of T-ALL that mediates T-cell transformation through transcriptional repression of its target genes. Our current understanding of the oncogenic properties downstream of TLX1 includes aneuploidy as a result of a deregulated mitotic checkpoint machinery,[4] T-cell differentiation arrest caused by repression of TCRα enhancer activity[26] and simultaneous inhibition of T-ALL tumor suppressor genes.[4,26] These studies provided important insights in the mechanisms that mediate T-cell transformation downstream of TLX1, but were solely focused on TLX1 binding at the promoter of direct target genes. Therefore, the functional consequences of genome-wide TLX1 binding in the context of human T-ALL development remained to be established.
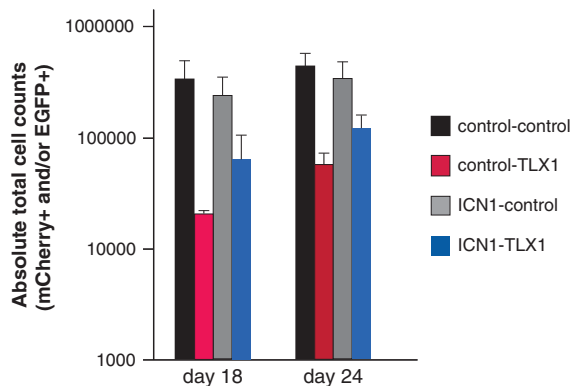

Figure 5. *Ex vivo* TLX1-ICN1 co-expression in human and mouse T-cell progenitor cells. Averaged absolute total cell counts of CD34+ progenitor T cells cultured from three independent donors on OP9-DLL1 for 18 or 24 days and transduced with either control vectors, a TLX1 overexpression, an ICN1 overexpression construct or TLX1 and ICN1 together.

Here, we report the genome-wide binding profile of TLX1 in human T-ALL and confirm ETS1 and RUNX1[7,26] as critical co-factors in TLX1 mediated transcriptional repression. Moreover, we identified clusters of high intensity TLX1 binding peaks at H3K27ac defined super-enhancers with broad binding of BRD4,[9] which were localized in the vicinity of genes that define the T-cell lineage identity. The concept of TLX1-driven repression of super-enhancers provides additional insights in the mechanisms that drive T-cell transformation downstream of TLX1, including global interference with T-cell differentiation and the V(D)J-recombination machinery by targeting enhancers near the TCR loci, *RAG1*, *RAG2* and *BCL11B*.

ETS1 and RUNX1 interact with NOTCH1 to regulate gene expression in both normal T-cell development and non-TLX1 driven T-ALL and key components of the NOTCH1 transcriptional program are driven by super-enhancer sequences.[9,10] Therefore, we subsequently explored the presumed cooperative relationship between TLX1 and NOTCH1. Integration of TLX1, ICN1, ETS1 and RUNX1 binding patterns with transcriptional read-out in T-ALL revealed an unprecedented transcriptional antagonism between TLX1 and NOTCH1, including TLX1-driven repression of the canonical NOTCH1 targets *NOTCH3*, *IGLL1*, *WNK2*, *SHQ1*, *c-MYC* and *IL7R*. Interestingly, TLX1 mediated repression of the *IL7R* gene occurred at the recently described distal super-enhancer[9] that is co-occupied by ICN1, RUNX1, ETS1 and BRD4. In line with this notion, ectopic *TLX1* expression in CD34+ human thymic precursor T cells caused significant downregulation of NOTCH1 target genes including reduced IL7R-alpha (CD127) surface expression.

Although transcriptional antagonism between cooperative T-ALL oncogenes seems counterintuitive, it provides intriguing new insights in the multi-step pathogenesis of TLX1-driven human leukemia. The model that emerges from our results is that ectopic expression of TLX1 would hijack ETS1 and RUNX1 functionality in the context of T-cell development. At a genome-wide level, this would trigger inhibition of enhancer activity, repression of key components of the NOTCH1 transcriptional program and global interference with normal T-cell differentiation and the V(D)J-recombination machinery. These oncogenic properties would eventually results in a pre-leukemic phenotype reminiscent of the thymic regression observed in murine TLX1 tumor models and drive T-cell maturation arrest. At the level of secondary genetic lesions required for full malignant transformation, this model implies a strong genetic pressure for acquiring activating *NOTCH1* mutations to overcome the initial TLX1 mediated suppression of NOTCH1 signaling, which is in line with the high frequency of gain-of-function *NOTCH1* mutations in human[14] and murine[4,5] TLX1-driven T-ALL. Moreover, broad TLX1 mediated downregulation of an extensive network of T-ALL tumor suppressor genes provides additional genetic pressure to reinforce tumor suppressor gene inactivation by genomic deletions or mutations during tumor progression in TLX1-positive leukemias. Notably, this model differs from the classical concept of the multi-step pathogenesis of

Figure 4. Ectopic TLX1 expression broadly interferes with the normal T-cell differentiation program. (**a**) Schematic overview of the workflow used for retroviral infection of human thymic CD34^{+} progenitor T cells with a TLX1 overexpression construct followed by immunophenotypic and transcriptional characterization upon *in vitro* culturing on a feeder layer of OP9 stromal cells expressing the NOTCH1 ligand DLL1, (**b**) Bar plot showing the averaged absolute counts of EGFP-positive CD34^{+} T-cell progenitors of three independent donors 6, 12 and 18 days post infection on the *in vitro* OP9-DLL1 co-culture system. (**c**) Flow-cytometry profiles of CD34^{+} progenitor T cells 12 days post transduction (representative example shown for three replicates) showing a CD4^{+}CD8^{+} stage arrest of T-cell progenitors ectopically expressing TLX1, (**d**) Flow-cytometry profile showing a drastic reduction in the percentage of IL7Rα surface positive (CD127^{+}) T-cell progenitors ectopically expressing TLX1, (**e**) TLX1 binding profile to loci critically involved in T-cell development including *TCR loci*, *RAG1* and *IL7R*, (**f**) CD34^{+} T-cell progenitors (two independent donors) transduced either with empty vector or with the TLX1 overexpression construct were profiled on a custom Agilent micro-array platform (see also Materials and methods). The average relative expression percentages in CD34^{+} thymocytes transduced with empty vector versus CD34^{+} T-cell progenitors ectopically expressing TLX1 from both independent experiments are shown for *NOTCH1*, *NOTCH3*, *IL7R*, *IGLL1*, *SHQ1* and *RAG1*, (**g**) RT-qPCR profiles of *IL7R* and *RAG2* confirming upregulated expression of these genes upon TLX1 knockdown in ALL-SIL.
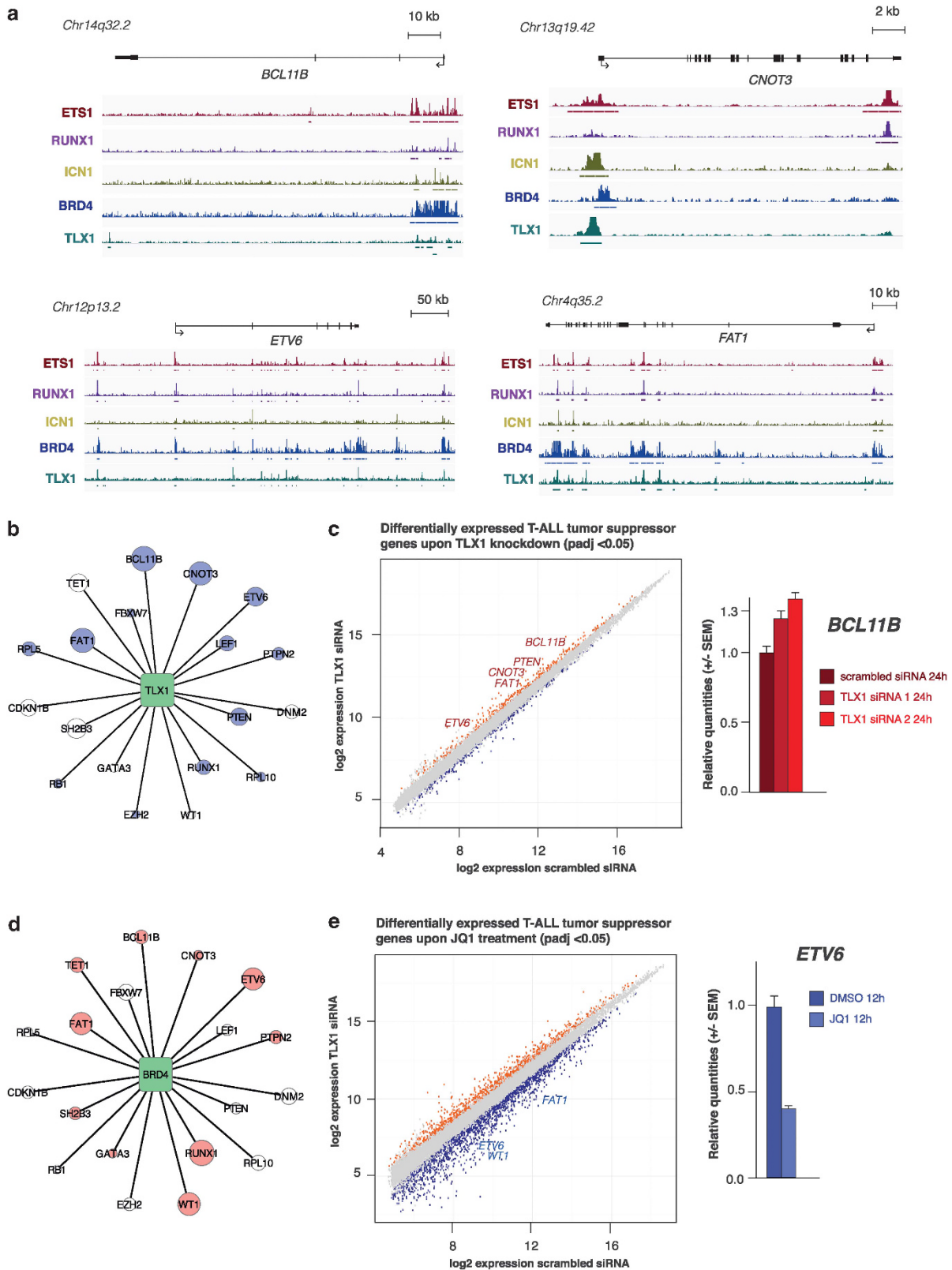
Figure 6. T-ALL tumor suppressor genes in the TLX1 regulatory network. (**a**) TLX1 ChIP-seq binding profiles at the known T-ALL tumor suppressor genes *BCL11B*, *CNOT3*, *ETV6* and *FAT1*, (**b**) Schematic overview with nodes of TLX1-bound tumor suppressor genes. Tumor suppressors that are upregulated upon TLX1 knockdown in ALL-SIL are shown in blue and the size of the node corresponds to the respective fold change, (**c**) Scatter plot indicating the tumor suppressor genes significantly upregulated upon TLX1 knockdown and confirmation of *BCL11B* upregulation by RT-qPCR, (**d**) Similar overview as (**b**). Tumor suppressors that are downregulated upon JQ1 treatment in ALL-SIL are shown in red and the size of the node corresponds to the respective fold change, (**e**) Scatter plot indicating significantly differentially expressed tumor suppressor genes in ALL-SIL upon JQ1 exposure.

T-ALL in which cooperative oncogenes and tumor suppressors alter proliferation, differentiation and survival of thymic precursor cells and expand the oncogenic phenotype of the developing tumor cell in a stepwise manner. Nevertheless, this particular model should be further confirmed beyond the use of T-ALL cell lines by analyzing the genome-wide TLX1 binding pattern in patient-derived T-ALL xenografts.

All together, our results uncover novel mechanistic insights in the role of TLX1 during the earliest stages of T-cell transformation and illustrate the power of integrative genomic analyses to understand the multi-step pathogenesis of TLX1 driven human leukemia.

CONFLICT OF INTEREST

The authors declare no conflict of interest.

AUTHOR CONTRIBUTIONS

KD performed and analyzed experiments and wrote the paper. WVL and MO performed bioinformatics on large-scale data sets. JVdM, IVdW, PR, AW and CEdB performed experiments. JC, JS, BP, NVR, TT, FS and PVV designed the experiments, directed research, analyzed data and wrote the paper. All the authors read and edited the manuscript.

REFERENCES

1 Ferrando AA, Neuberg DS, Dodge RK, Paietta E, Larson RA, Wiernik PH et al. Prognostic importance of TLX1 (HOX11) oncogene expression in adults with T-cell acute lymphoblastic leukaemia. Lancet 2004; 363: 535–536.

2 Hawley RG, Fong AZ, Reis MD, Zhang N, Lu M, Hawley TS. Transforming function of the HOX11/TCL3 homeobox gene. Cancer Res 1997; 57: 337–345.

3 Hawley RG, Fong AZ, Lu M, Hawley TS. The HOX11 homeobox-containing gene of human leukemia immortalizes murine hematopoietic precursors. Oncogene 1994; 9: 1–12.

4 De Keersmaecker K, Real PJ, Gatta GD, Palomero T, Sulis ML, Tosello V et al. The TLX1 oncogene drives aneuploidy in T cell transformation. Nat Med 2010; 16: 1321–1327.

5 Rakowski LA, Lehotzky EA, Chiang MY. Transient responses to NOTCH and TLX1/HOX11 inhibition in T-cell acute lymphoblastic leukemia/lymphoma. PLoS ONE 2011; 6: e16761.

6 Owens BM, Hawley TS, Spain LM, Kerkel KA, Hawley RG. TLX1/HOX11-mediated disruption of primary thymocyte differentiation prior to the CD4+CD8+ double-positive stage. Br J Haematol 2006; 132: 216–229.

7 Dadi S, Le Noir S, Payet-Bornet D, Lhermitte L, Zacarias-Cabeza J, Bergeron J et al. TLX homeodomain oncogenes mediate T cell maturation arrest in T-ALL via interaction with ETS1 and suppression of TCRalpha gene expression. Cancer Cell 2012; 21: 563–576.

8 Weng AP, Ferrando AA, Lee W, Morris JPt, Silverman LB, Sanchez-Irizarry C et al. Activating mutations of NOTCH1 in human T cell acute lymphoblastic leukemia. Science 2004; 306: 269–271.

9 Wang H, Zang C, Taing L, Arnett KL, Wong YJ, Pear WS et al. NOTCH1-RBPJ complexes drive target gene expression through dynamic interactions with superenhancers. Proc Natl Acad Sci USA 2014; 111: 705–710.

10 Wang H, Zou J, Zhao B, Johannsen E, Ashworth T, Wong H et al. Genome-wide analysis reveals conserved and divergent features of Notch1/RBPJ binding in human and murine T-lymphoblastic leukemia cells. Proc Natl Acad Sci USA 2011; 108: 14908–14913.

11 Hnisz D, Abraham BJ, Lee TI, Lau A, Saint-Andre V, Sigova AA et al. Super-enhancers in the control of cell identity and disease. Cell 2013; 155: 934–947.

12 Whyte WA, Orlando DA, Hnisz D, Abraham BJ, Lin CY, Kagey MH et al. Master transcription factors and mediator establish super-enhancers at key cell identity genes. Cell 2013; 153: 307–319.

13 Loven J, Hoke HA, Lin CY, Lau A, Orlando DA, Vakoc CR et al. Selective inhibition of tumor oncogenes by disruption of super-enhancers. Cell 2013; 153: 320–334.

14 Asnafi V, Buzyn A, Le Noir S, Baleydier F, Simon A, Beldjord K et al. NOTCH1/FBXW7 mutation identifies a large subgroup with favorable outcome in adult T-cell acute lymphoblastic leukemia (T-ALL): a Group for Research on Adult Acute Lymphoblastic Leukemia (GRAALL) study. Blood 2009; 113: 3918–3924.

15 Clappier E, Gerby B, Sigaux F, Delord M, Touzri F, Hernandez L et al. Clonal selection in xenografted human T cell acute lymphoblastic leukemia recapitulates gain of malignancy at relapse. J Exp Med 2011; 208: 653–661.

16 Volders PJ, Helsens K, Wang X, Menten B, Martens L, Gevaert K et al. LNCipedia: a database for annotated human lncRNA transcript sequences and structures. Nucleic Acids Res 2013; 41: D246–D251.

17 Lee TI, Johnstone SE, Young RA. Chromatin immunoprecipitation and microarray-based analysis of protein location. Nat Protoc 2006; 1: 729–748.

18 Langmead B, Trapnell C, Pop M, Salzberg SL. Ultrafast and memory-efficient alignment of short DNA sequences to the human genome. Genome Biol 2009; 10: R25.

19 Feng J, Liu T, Zhang Y. Using MACS to identify peaks from ChIP-Seq data. Curr Protoc Bioinformatics 2011; Chapter 2: Unit 2.14.

20 Quinlan AR, Hall IM. BEDTools: a flexible suite of utilities for comparing genomic features. Bioinformatics 2010; 26: 841–842.

21 Machanick P, Bailey TL. MEME-ChIP: motif analysis of large DNA datasets. Bioinformatics 2011; 27: 1696–1697.

22 Heinz S, Benner C, Spann N, Bertolino E, Lin YC, Laslo P et al. Simple combinations of lineage-determining transcription factors prime cis-regulatory elements required for macrophage and B cell identities. Mol Cell 2010; 38: 576–589.

23 Van de Walle I, Waegemans E, De Medts J, De Smet G, De Smedt M, Snauwaert S et al. Specific Notch receptor-ligand interactions control human TCR-alphabeta/gammadelta development by inducing differential Notch signal strength. J Exp Med 2013; 210: 683–697.

24 Van de Walle I, De Smet G, Gartner M, De Smedt M, Waegemans E, Vandekerckhove B et al. Jagged2 acts as a Delta-like Notch ligand during early hematopoietic cell fate decisions. Blood 2011; 117: 4449–4459.

25 Della Gatta G, Palomero T, Perez-Garcia A, Ambesi-Impiombato A, Bansal M, Carpenter ZW et al. Reverse engineering of TLX oncogenic transcriptional networks identifies RUNX1 as tumor suppressor in T-ALL. Nat Med 2012; 18: 436–440.

26 Allen TD, Zhu YX, Hawley TS, Hawley RG. TALE homeoproteins as HOX11-interacting partners in T-cell leukemia. Leuk Lymphoma 2000; 39: 241–256.

27 Milech N, Gottardo NG, Ford J, D'Souza D, Greene WK, Kees UR et al. MEIS proteins as partners of the TLX1/HOX11 oncoprotein. Leuk Res 2010; 34: 358–363.

28 Filippakopoulos P, Qi J, Picaud S, Shen Y, Smith WB, Fedorov O et al. Selective inhibition of BET bromodomains. Nature 2010; 468: 1067–1073.

29 Durinck K, Wallaert A, Van de Walle I, Van Loocke W, Volders PJ, Vanhauwaert S et al. The Notch driven long non-coding RNA repertoire in T-cell acute lymphoblastic leukemia. Haematologica 2014; 99: 1808–1816.

30 Herranz D, Ambesi-Impiombato A, Palomero T, Schnell SA, Belver L, Wendorff AA et al. A NOTCH1-driven MYC enhancer promotes T cell development, transformation and acute lymphoblastic leukemia. Nat Med 2014; 20: 1130–1137.

Supplementary Information accompanies this paper on the Leukemia website (http://www.nature.com/leu)